SHRIMP U–Pb zircon geochronology of Neoproterozoic crustal granitoids (Southern Brazil): A case for discrimination of emplacement and inherited ages

Luiz Carlos da Silva[a,c,*], Neal Jesse McNaughton[b], Ian R. Fletcher[b]

[a]*Geological Survey of Brazil-CPRM, SGAN 603, 1° Andar, 70830-039, Brasília DF, Brazil*
[b]*Centre for Global Metallogeny, School of Earth and Geographical Sciences, The University of Western Australia, Nedlands 6009, Australia*
[c]*Instituto de Geociências, Universidade de Brasília/UnB, Brazil*

Abstract

SHRIMP U–Pb zircon studies on two post-collisional granitic plutons and reassessment of the data previously reported for two anatectic gneissic granites are used to assess the late Neoproterozoic history of the Florianópolis Batholith, southern Brazil. The results, supported by SEM backscattered and cathodoluminescence imagery, identify inherited zircon populations and confirm the long-lived, crustal recycling processes responsible for the accretion of the batholith. The study casts new lights on the timing of the processes involved in the generation and modification of the internal structure of distinct zircon populations, and enables discrimination to be made between inherited cores and melt-precipitated overgrowths. New dating of two post-tectonic plutons (samples 1 and 2) revealed crystals showing magmatic-textured cores sharply bounded by melt-precipitated overgrowths. The U/Pb isotopic results from both samples spread along concordia by ca. 40 m.y. (sample 1) to 100 m.y. (sample 2), clustering in two closely spaced (bimodal), partially overlapping peaks. Melt-precipitated rims and homogeneous new grains, dated at ca. 600 Ma, furnish the crystallisation age of the plutons. The magmatic textured cores and xenocrysts dated at ca. 630–620 Ma are interpreted as inherited restitic material from supposedly short-lived (meta)granitic sources. The reassessment of previous SHRIMP data of two banded anatectic granitoids (samples 3 and 4) revealed more complex morphological patterns, in which the overgrown inherited cores are sharply bounded against large melt-precipitated rims, dated at ca. 600 Ma and 592±2 Ma, respectively. Major populations of magmatic-textured inherited cores dated at 2006±3 Ma and 2175±13 Ma characterise samples 3 and 4, respectively. The latter additionally shows metamorphic and magmatic inherited cores with a large range of ages (ca. 2900–620 Ma), suggesting partial melting of metasedimentary components. The main magmatic Paleoproterozoic core populations are interpreted as inherited restite from partial melting of the adjacent (meta)tonalitic gneiss and amphibolitic country-rock (paleosome). The recognition of the (melt-precipitated) Neoproterozoic overgrowths and new crystals, and the restite provenance of the cores, supplants a previous interpretation of Paleoproterozoic magmatism (cores) and Neoproterozoic (solid-state) metamorphic overprint. As a major consequence of the former

---

* Corresponding author. Geological Survey of Brazil-CPRM, SGAN 603, 1° Andar, 70830-039, Brasília DF, Brazil. Tel.: +55 61 2231166; fax: +55 61 2241616.

E-mail address: luizcarlos@df.cprm.gov.br (L.C. da Silva).

interpretation, the unit was mistakenly considered part of major Paleoproterozoic gneissic remnant within the Neoproterozoic Florianópolis Batholith/arc.

1. Introduction

Partial melting of ancient basement giving rise to new granitoid melts is a common feature in many continental magmatic arcs and collisional orogens. Poldevaart's (1955, 1956) pioneering studies (as quoted by Hanchar and Miller, 1993) showed how zircon could be used to distinguish between growth processes, for example to distinguish between pre-magmatic cores surrounded by magmatic overgrowths. The use of SEM (scanning electron microscopy), by means of backscattered (BSE) and cathodoluminescence (CL) imaging, coupled with sensitive high-resolution ion microprobe mass spectrometer (SHRIMP) analyses has refined this petrologic tool. Accordingly, the occurrences of crystals with old cores, rimmed by magmatic overgrowths have been revealed in numerous granitic rocks worldwide (e.g. Hanchar and Miller, 1993; Williams, 1998). Studies of mid-Paleozoic S-type granites led Williams (1998) to regard the core-overgrowth texture to be a general feature of crustal-derived S-type granites. U–Pb isotopic analyses of domains within zircon grains should reveal the time of the magma crystallization (overgrowth) and granitic source (un-melted restitic material in the cores) (Williams, 1998). Typically, only zircon provides this insight into the nature and age of the granitic source. Discriminating and determining precise ages of inheritance and new melt-precipitated overgrowths is, therefore, one of the major tasks for dating crustal anatectic granitoids and migmatites. Meeting this challenge requires correct interpretation of SEM imagery, relating each domain to a particular petrogenetic process, and precise in situ dating.

The Florianópolis Batholith is a major component of the granitic continental arc from the Neoproterozoic Dom Feliciano Orogen/Mantiqueira Province (Fig. 1). Within the batholith some syn- to late tectonic plutons are comprised of granites with large amounts of unmelted restitic material (migmatites). Even among
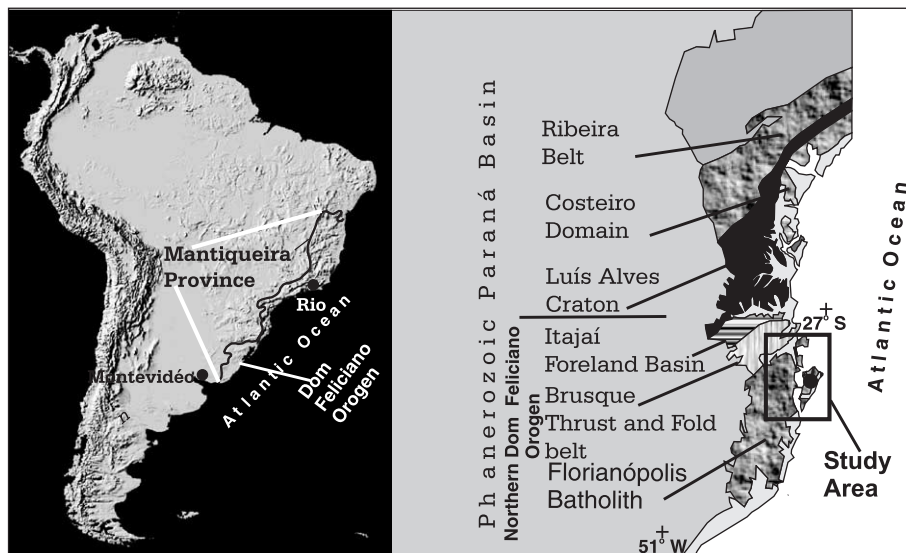
Fig. 1. Location map of the study area displaying the Florianópolis Batholith in the framework of the southern Mantiqueira Province/Dom Feliciano Orogen.

the more evolved homogeneous post-tectonic intrusions good preservation of restitic zircons may be locally observed. We have dated through SHRIMP U–Pb zircon systematics two of these post-tectonic crustal-derived Neoproterozoic homogeneous plutons (samples 1 and 2). Sample 1 (S1) comes from an A2-type (sensu Eby, 1992), and sample 2 (S2) is from an I-Caledonian-type granite (sensu Pitcher, 1983) minor intrusive body. Two other late tectonic, banded anatectic leucosomes (granitoids), previously studied through SHRIMP U–Pb zircon systematics (Silva et al., 2000), are re-investigated in the present study (samples 3 and 4). Both samples are characterized by zircon populations dominantly with large magmatically-zoned cores sharply bounded against thin melt-precipitated euhedral Neoproterozoic rims.

Previous SHRIMP U–Pb zircon studies of Silva et al. (2000) and Hartmann et al. (2000), supported by ID-TIMS U–Pb zircon data from Babinski et al. (1997), considered the main pooled magmatic cores population from S3 and S4 to have crystallisation Paleoproterozoic ages whereas the Neoproterozoic melt-precipitated rims were interpreted as resulting from a solid-state (metamorphic) overprinting. Basei (2000), using ID-TIMS, and Silva et al. (2002), through SHRIMP U–Pb zircon systematics, dated another facies of the anatectic rock and presented results that challenged this interpretation. They interpreted the overgrowths as melt-precipitated Neoproterozoic phases and hence the crystallisation age of the rock was ascribed to a Neoproterozoic event.

The present study is based on new SEM imagery, new SHRIMP data for S1 and S2, and by the re-interpretation of the data previously obtained by Silva et al. (2000) on S3 and S4. It provides consistent new imaging criteria for distinguishing multiple generations of inherited (magmatic) and metamorphic cores, as well as melt-precipitated overgrowths zircon.

2. Florianópolis Batholith

The 650–600 Ma Florianópolis Batholith constitutes the northern tip of the Dom Feliciano Orogen/Belt, ascribed to the Brasiliano system of orogens in southern Brazil. The batholith is about 200 km long and 60 km wide is Santa Catarina State (Figs. 1 and 2) and is part of a major Neoproterozoic magmatic arc (Fig. 1).

Modal compositions of the main batholithic phases are extremely uniform. Silva (1999) demonstrated that most of the plutons are post-tectonic, metaluminous, leucocratic, highly silicic ($SiO_2 > 68\%$), with an overwhelming dominance of granite (s.s.) compositions (fields 3a and 3b of Streckeisen, 1976), belonging to the high-K calc-alkaline series, corresponding to I-Caledonian plutons (sensu Pitcher, 1983). Minor plutons include Eby's (1992) subalkalic A_2 types and minor shoshonitic and alkaline phases (Chemale et al., 2003). About 20% of the exposed area comprises syn-tectonic, strike-slip related Neoproterozoic plutons, as well as partially melted Paleoproterozoic remnants of migmatitic orthogneisses and amphibolites, intruded by the post-tectonic plutons. In addition to these petrological characteristics, the Sm–Nd signature dominated by highly negative ε_{Nd} values and Meso and Paleoproterozoic T_{DM} model-ages ($T=600$ Ma) indicates that the batholith is part of a mature intracontinental magmatic arc (e.g. Silva, 1999).

Within highly assimilated megaxenoliths (paleosomes/protoliths), the oldest preserved granitic (metatonalite) phase (G_1 in the local granitic chronostratigraphy) shows several pulses of in situ anatexis, giving rise to abundant leucosomes (G_2) and major plutons of banded granitoid (Figs. 3, 4 and 12). Abundant post-tectonic (G_3) granitic phases cut the migmatitic complex and contain many megaxenoliths of the association of G_1+G_2 (Figs. 3 and 12). The G_1 gneissic tonalite, and partially melted amphibolite remnants form metre- to decimetre-sized xenoliths, whereas G_2 banded granitoid neosomes (migmatites) are the most voluminous and tend to contain many partly assimilated xenoliths and restites of their tonalitic and amphibolitic country rock (G_1) (Figs. 3, 4 and 12).

The anatectic granites are characterized by a penetrative sub-horizontal flow banding related to the latest compressive stages of the orogen (late-tectonic melting), showing sharp cross-cutting relationships with the gneissic banding of the country-rock. Very pronounced regional strike-slip related NE-trending shear zones cut the unit but do not significantly affect the investigated outcrops.

The migmatitic association is ascribed to the Camboriú and Águas Mornas migmatite complexes (Fig. 2). It is interpreted as the exposed roots of the batholith, partially melted during the orogenic metamorphic peak, exhumed and later intruded by the
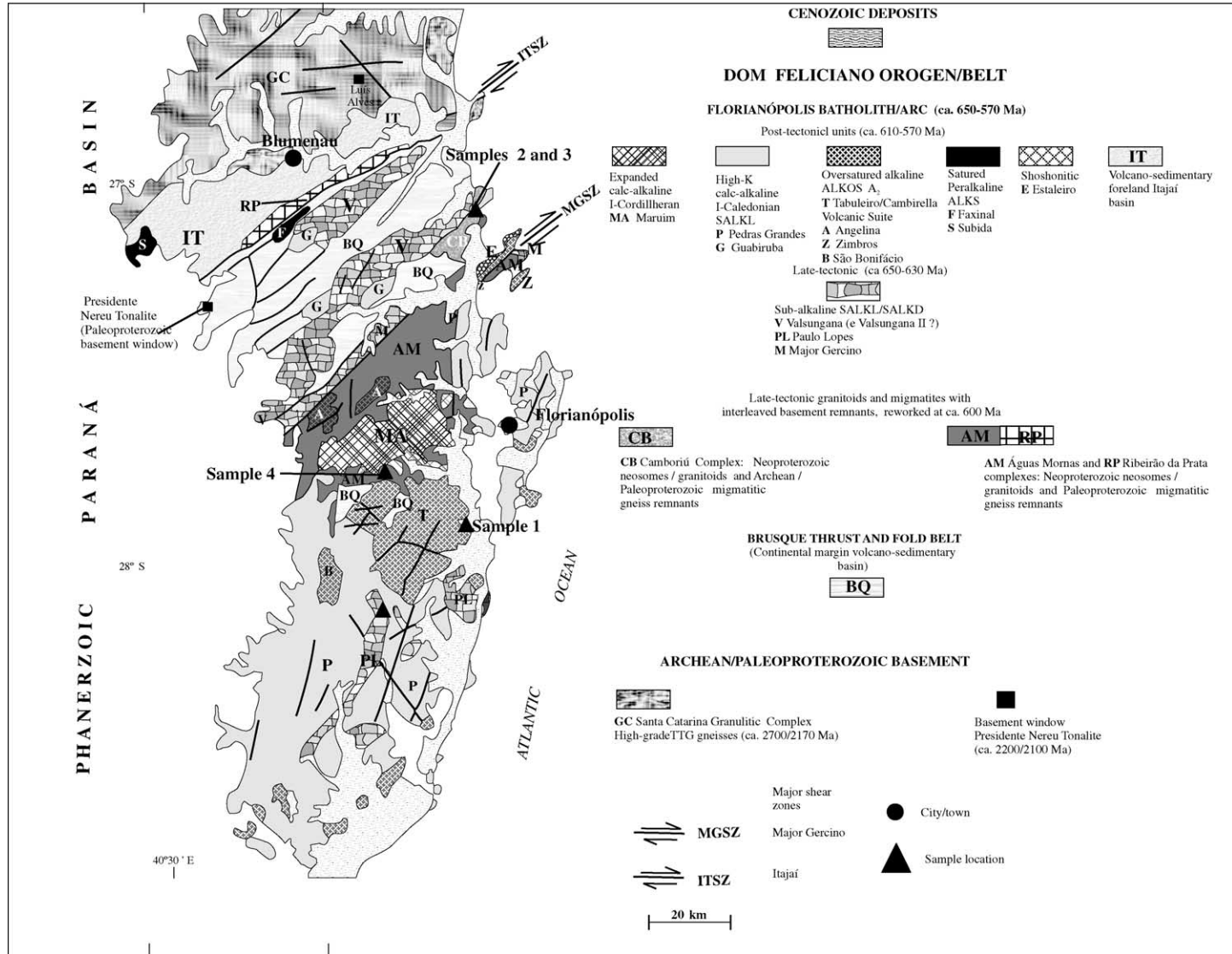
Fig. 2. Simplified geologic map of the Florianópolis Batholith and other units from the Dom Feliciano Orogen in the context of Santa Catarina Precambrian Shield (based on Silva et al., 2003).
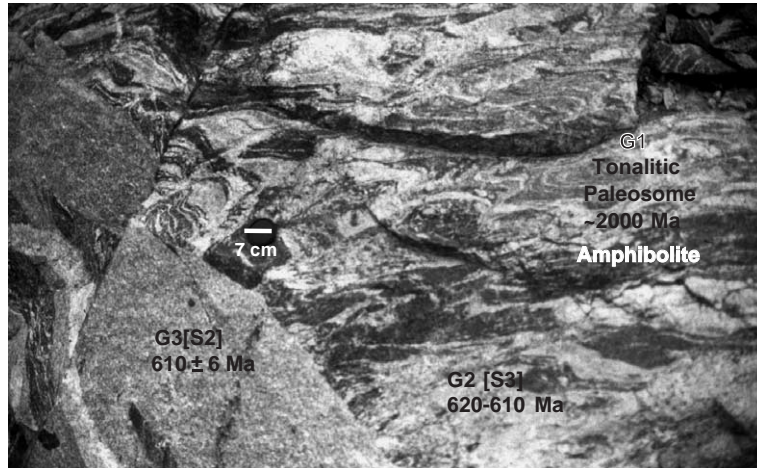
Fig. 3. Polyphase migmatitic gneiss (Banded anatectic granite/Camboriú Complex) at S3 and S4 sample sites (Caseca Quarry), featuring cross-cutting intrusive relations of dated the G_3 post-tectonic Guabiruba Granite (medium gray) with the dated G_2, banded anatectic gneiss (light gray). The granite is slight foliated and is clearly discordant to the earlier G_2 gneissic fabric. The complex folded G_1 tonalitic remnants (dark gray paleosome) show abundant white, concordant (in situ) and injected leucosome bands and pockets. Note the presence of preserved amphibolite bands discretely injected by G_2.

post-tectonic batholithic phases from ca. 600 to 580 Ma, the main period of granitic magmatism.

3. New SHRIMP U–Pb data on the post-tectonic granitoids (S1 and S2)

The location, geology and petrogenesis of the post-tectonic granites (samples 1 and 2) are described in detail in Appendix A.

3.1. Zircon morphology and U–Th–Pb results from S1 and S2

Zircon populations from both samples are morphologically similar. BSE/CL images reveal crystals with euhedral prismatic habit, mostly with low aspect ratios (~2:1) (S1, Fig. 5A, B, C, E), or with length/width ratio of 3:1 (S2, Fig. 7A–F), typical of magmatic crystallisation. Some crystals are homogeneous (without core/rim separation) presenting fine-scale oscil-
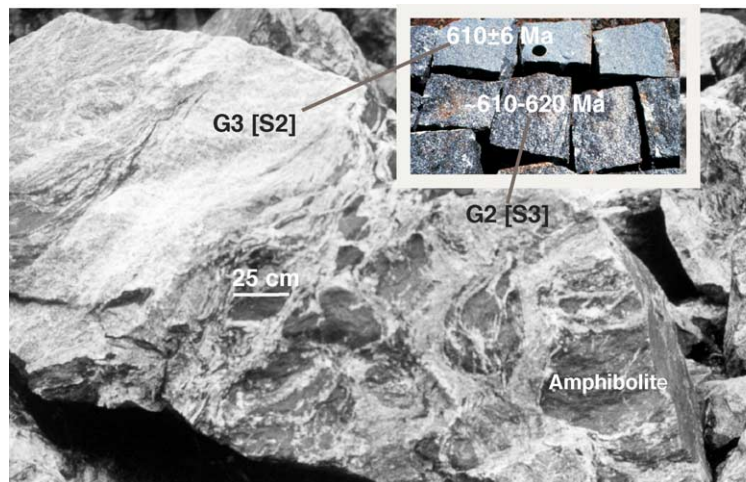
Fig. 4. Polyphase migmatitic gneiss from Camboriú Complex at S3 and S4 sample site (Caseca Quarry), showing the same structural relations as Fig. 3 and the blocks collected for analyses.
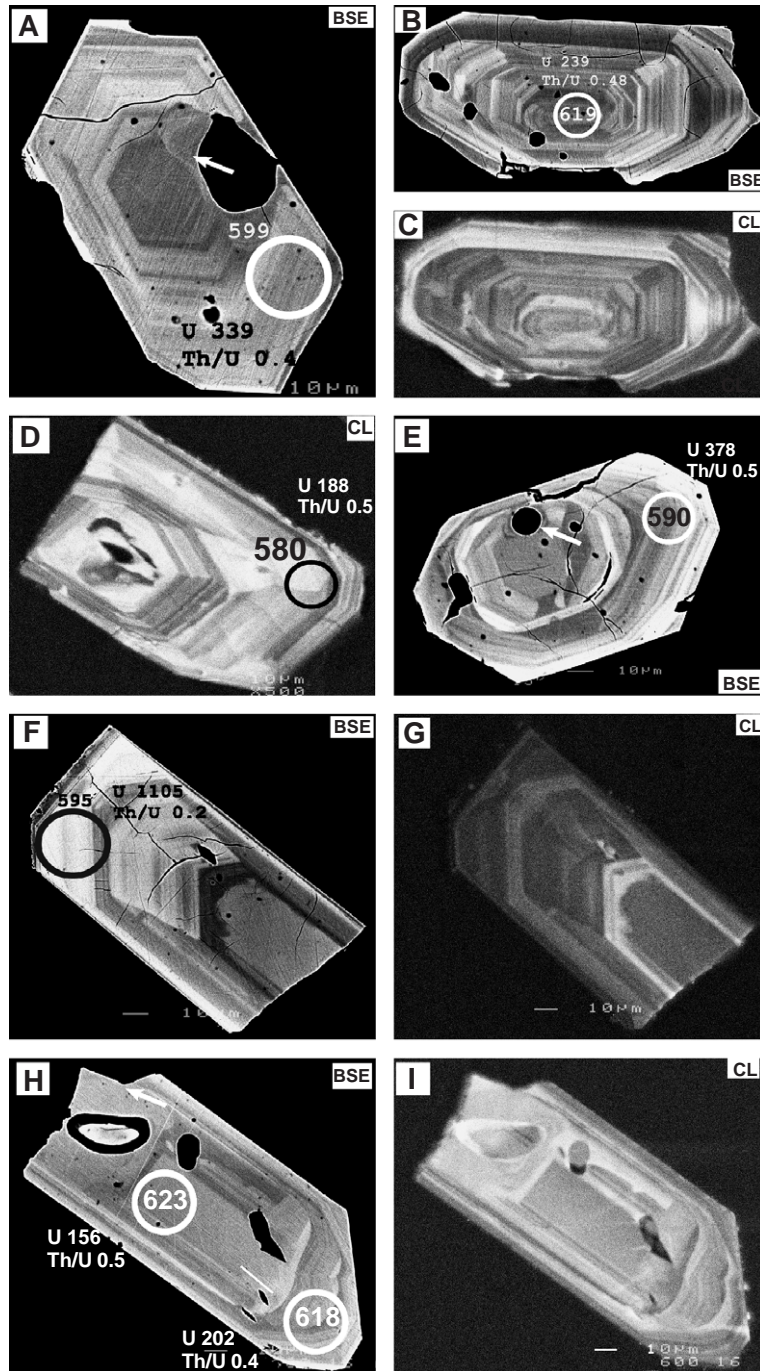
Fig. 5. Backscattered electron (BSE) and cathodoluminescence (CL) images of zircons from the sample 1 (Tabuleiro Granite). Crystals numbering follows Table 1. (A) Crystal 14; (B–C) Crystal 8; (D) Crystal 23; (E) Crystal 21; (F–G) Crystal 22; (H–I) Crystal 9. Arrow=halo around mineral inclusions. Circles (~30 μm)=SHRIMP spot location. Ages indicated in Ma; U in ppm.

latory zoned, or complex-zoned magmatic textures. Most crystals show an internal morphology characterized by sharp discrimination between external, euhedral, melt-precipitated overgrowths and magmatic-textured cores.

The U and Th contents and Th/U ratios from cores and overgrowths (which mostly range from 0.1 to 0.8; Tables 1 and 2) are characteristic of felsic magmatic rocks (e.g. Gebauer et al., 1997). A few overgrowths are U-enriched, up to ca. 1100 ppm (S1, Fig. 5F) and ca. 1500 ppm (S2, Fig. 7D). As these analyses also have high Th, they preserve high (magmatic) Th/U ratios. These domains are recognized as bright BSE, CL-dark domains and are accompanied by fracturing in radial or concentric patterns due to expansion by metamictization. S2 presents some crystals with relatively low-U contents, and consequently higher Th/U ratios (~1.3) (Fig. 7B,C). The analytical data are given in Tables 1 and 2 and shown in the concordia plots in Figs. 6 (S1) and 8 (S2).

The age data from both samples spread almost continuously from ca. 580 Ma to ca. 620 Ma (S1, Fig. 6) and from ca. 570 Ma to ca. 670 Ma (S2, Fig. 8) and form two closely spaced (bimodal), partially overlapped pooled ages peaks, clustering at ca. 600–620 Ma (S1) and ca. 610–630 Ma (S2). Each one of these clusters is ascribed to a particular morphologic population: melt-precipitated rims and new crystals (Group 1, the younger group) and magmatic inherited cores and xencrysts (Group 2).

Group 1 domains comprise discrete, magmatic-textured (oscillatory-zoned) euhedral grains, and magmatic-textured (oscillatory-zoned) overgrowths. Both present typical magmatic U and Th contents and Th/U ratios (Figs. 5 and 7, Tables 1 and 2). As observed in several crystals, some domains show haloes around mineral inclusions seen as light areas in BSE (arrow in Fig. 5A S3). These bright BSE domains may also be seen as discordant, irregular rims of smooth scalloped (undated) overgrowth, characteristic of magmatic corrosion of the overgrown core (e.g. Hanchar and Miller, 1993) ("ov" in Fig. 7G, S2). Owing to these characteristics, this group is interpreted as a new magmatic melt-precipitated zircon phase.

Group 2 domains show magmatic (oscillatory-zoned) and sector zoning, or may be unzoned, with magmatic U and Th contents and Th/U ratios,

ranging mostly from 0.2 to 0.8 (Tables 1 and 2, Figs. 5 and 7). The rest of the Group 2 comprises minor, discrete, (inherited) xenocrystic crystals with fine-scale, magmatic oscillatory zoning and magmatic Th/U ratios mostly ranging from 0.2 to 0.8 (Tables 1 and 2).

3.1.1. $^{206}Pb/^{238}U$ ages from the Tabuleiro Granite (S1)

Group 1 analyses (melt-precipitated overgrowths and magmatic new crystals) form a single cluster (n=7), corresponding to a homogeneous population with no scatter of a geological nature (χ^2=0.7) and with an age of 597±9 Ma (light grey error boxes in Fig. 6). This result is interpreted as the crystallisation age of the pluton. The only discarded analyses are #26-1 (Fig. 6, Table 1), which is a mixed core/rim domain, and discordant analyses (blank error boxes in Fig. 6).

Group 2 analyses (inherited magmatic cores and crystals) were obtained on 6 spots (Fig. 6). They form a single cluster, corresponding to a homogeneous population with little scatter of a geological nature (χ^2=0.5) and with an apparent age of 617±9 Ma (dark error boxes on Fig. 6). This population is ~20 m.y. older than the ca. 597 Ma Group 1, and is interpreted as a zircon component inherited from a paleosomatic granitic source previous dated at ca. 630 Ma, partially melted at ca. 597 Ma.

3.1.2. $^{206}Pb/^{238}U$ ages from the Guabiruba Granite (S2)

Nineteen analyses (Group 1) from melt-precipitated overgrowths and magmatic new crystals are shown in Fig. 8 and Table 2. These Group 1 analyses also represent a single data population with litle detectable geological scatter (mean χ^2=1.1). and yielded an age of 610±6 Ma (light gray error boxes, Fig. 8), interpreted as the crystallization age of the pluton. Disregarded data include spot #19-2, interpreted to be from a domain that has experienced recent Pb-loss, spot #24-1, from a morphologically distinct crystal, and discordant analyses (blank error boxes in Fig. 8).

Group 2 analyses (inherited magmatic cores and crystals) comprise 11 spots (Fig. 8, Table 2). As observed in S1, they form a single, morphologically uniform population with little scatter of a geological

Table 1
U–Pb–Th SHRIMP isotopic data from sample 1, Tabuleiro Granite

Grain-spot	U (ppm)	Th (ppm)	Th/U	f ^{206}Pb (%)	Ratios corrected for common Pb					% conc.	^{206}Pb*/^{238}U Age (Ma)
					^{207}Pb*/^{206}Pb*	^{208}Pb*/^{206}Pb*	^{206}Pb*/^{238}U	^{207}Pb*/^{235}U	^{208}Pb*/^{232}Th		
1-1	**437**	**33**	**0.08**	**−0.003**	**0.0637±0.0014**	**0.0311±0.0028**	**0.1011±0.0010**	**0.888±0.022**	**0.0413±0.0038**	**85**	**621±6**
5-1	292	145	0.50	0.002	0.0595±0.0014	0.1502±0.0035	0.0994±0.0010	0.816±0.022	0.0301±0.0008	104	611±6
6-1	**390**	**172**	**0.44**	**0.001**	**0.0591±0.0015**	**0.1332±0.0035**	**0.0999±0.0010**	**0.814±0.023**	**0.0302±0.0009**	**107**	**614±6**
8-1	**239**	**116**	**0.48**	**0.001**	**0.0609±0.0023**	**0.1427±0.0055**	**0.1008±0.0011**	**0.847±0.035**	**0.0297±0.0012**	**97**	**619±6**
9-1	*202*	*90*	*0.45*	*0.003*	*0.0591±0.0021*	*0.1307±0.0050*	*0.1007±0.0011*	*0.820±0.032*	*0.0294±0.0012*	*108*	*618±6*
9-2	**156**	**93**	**0.59**	**0.000**	**0.0616±0.0014**	**0.1787±0.0038**	**0.1014±0.0011**	**0.861±0.023**	**0.0305±0.0008**	**95**	**623±6**
10-1	274	122	0.45	0.001	0.0619±0.0017	0.1410±0.0041	0.0959±0.0010	0.819±0.025	0.0303±0.0009	88	590±6
11-1	1302	496	0.38	0.002	0.0597±0.0005	0.0968±0.0011	0.0913±0.0009	0.752±0.011	0.0232±0.0004	95	563±5
12-1	**217**	**96**	**0.44**	**0.001**	**0.0603±0.0018**	**0.1298±0.0043**	**0.0973±0.0010**	**0.810±0.027**	**0.0286±0.0010**	**97**	**599±6**
12-2	**217**	**94**	**0.43**	**0.003**	**0.0569±0.0024**	**0.1224±0.0056**	**0.0996±0.0011**	**0.782±0.035**	**0.0282±0.0013**	**125**	**612±6**
13-1	165	128	0.78	0.024	0.0683±0.0053	0.2507±0.0126	0.0964±0.0011	0.908±0.072	0.0311±0.0016	68	593±7
14-1	339	150	0.44	0.000	0.0597±0.0009	0.1359±0.0021	0.0974±0.0010	0.801±0.015	0.0298±0.0006	101	599±6
15-1	**631**	**318**	**0.50**	**0.001**	**0.0598±0.0013**	**0.1535±0.0032**	**0.1014±0.0010**	**0.835±0.021**	**0.0309±0.0007**	**105**	**623±6**
16-1	291	175	0.60	0.001	0.0598±0.0010	0.1850±0.0028	0.0984±0.0010	0.811±0.017	0.0302±0.0006	102	605±6
17-1	**433**	**225**	**0.52**	**0.001**	**0.0591±0.0012**	**0.1582±0.0030**	**0.0999±0.0010**	**0.815±0.020**	**0.0304±0.0007**	**108**	**614±6**
18-1	**512**	**231**	**0.45**	**−0.001**	**0.0620±0.0010**	**0.1412±0.0023**	**0.0956±0.0010**	**0.818±0.016**	**0.0299±0.0006**	**87**	**589±6**
20-1	355	157	0.44	0.002	0.0587±0.0011	0.1264±0.0026	0.0963±0.0010	0.780±0.017	0.0275±0.0006	107	593±6
21-1	*378*	*179*	*0.47*	*0.001*	*0.0593±0.0010*	*0.1503±0.0025*	*0.0959±0.0010*	*0.784±0.016*	*0.0304±0.0006*	*102*	*590±6*
22-1	1105	277	0.25	0.001	0.0593±0.0005	0.0748±0.0010	0.0967±0.0010	0.791±0.011	0.0288±0.0005	103	595±6
23-1	*188*	*99*	*0.53*	*0.005*	*0.0572±0.0020*	*0.1530±0.0050*	*0.0942±0.0010*	*0.743±0.029*	*0.0273±0.0009*	*116*	*580±6*
24-1	2228	530	0.24	0.004	0.0577±0.0006	0.0718±0.0013	0.0666±0.0007	0.530±0.008	0.0201±0.0004	80	416±4
25-1	*306*	*178*	*0.58*	*0.000*	*0.0620±0.0008*	*0.1866±0.0022*	*0.0980±0.0010*	*0.837±0.014*	*0.0315±0.0005*	*90*	*602±6*
26-1	508	172	0.34	0.002	0.0587±0.0008	0.0996±0.0019	0.0945±0.0010	0.765±0.014	0.0277±0.0006	105	582±6

(UWA Mount 96-43 A).

f ^{206}Pb is the proportion of common Pb in ^{206}Pb, determined using the measured ^{206}Pb/^{208}Pb and Th/U ratios.

%conc. is concordance, as $100\{t[^{206}\text{Pb}/^{238}\text{U}]/t[^{207}\text{Pb}/^{206}\text{Pb}]\}$. Bold=cores, Italics=rims, Regular=homogeneous crystals, Underline=Mixed domain.

Table 2
U–Pb–Th SHRIMP isotopic data from sample 2, Guabiruba Granite

Grain-spot	U (ppm)	Th (ppm)	Th/U	f ^{206}Pb (%)	Ratios corrected for common Pb					% conc	^{206}Pb*/^{238}U Age (Ma)
					^{207}Pb*/^{206}Pb*	^{208}Pb*/^{206}Pb*	^{206}Pb*/^{238}U	^{207}Pb*/^{235}U	^{208}Pb*/^{232}Th		
1-1	**649**	**433**	**0.67**	**0.000**	**0.0610±0.0005**	**0.2029±0.0015**	**0.1019±0.0013**	**0.857±0.014**	**0.0310±0.0005**	**98**	**625±8**
1-2	**489**	**211**	**0.43**	**−0.001**	**0.0614±0.0008**	**0.1322±0.0019**	**0.1011±0.0013**	**0.855±0.017**	**0.0309±0.0006**	**95**	**621±8**
1-3	*657*	*33*	*0.05*	*0.003*	*0.0597±0.0008*	*0.0151±0.0016*	*0.0988±0.0013*	*0.814±0.016*	*0.0297±0.0033*	*102*	*607±8*
2-1	**513**	**217**	**0.42**	**0.004**	**0.0603±0.0010**	**0.1301±0.0025**	**0.1009±0.0013**	**0.838±0.019**	**0.0310±0.0007**	**101**	**620±8**
2-2	*548*	*224*	*0.41*	*0.026*	*0.0607±0.0021*	*0.1326±0.0049*	*0.0992±0.0013*	*0.830±0.032*	*0.0322±0.0013*	*97*	*610±8*
3-1	213	177	0.83	0.001	0.0601±0.0011	0.2502±0.0034	0.1006±0.0013	0.834±0.020	0.0303±0.0006	102	618±8
4-1	*245*	*19*	*0.08*	*0.000*	*0.0589±0.0012*	*0.0227±0.0023*	*0.0991±0.0014*	*0.804±0.020*	*0.0296±0.0031*	*108*	*609±8*
4-2	**339**	**881**	**2.60**	**−0.001**	**0.0611±0.0013**	**0.7893±0.0053**	**0.1022±0.0013**	**0.861±0.023**	**0.0310±0.0005**	**98**	**627±8**
4-3	*1534*	*55*	*0.04*	*0.027*	*0.0602±0.0012*	*0.0149±0.0027*	*0.0991±0.0013*	*0.823±0.021*	*0.0412±0.0076*	*99*	*609±8*
5-1	1330	727	0.55	0.004	0.0580±0.0007	0.1721±0.0018	0.0671±0.0009	0.536±0.010	0.0211±0.0004	79	418±5
6-1	**401**	**262**	**0.65**	**0.002**	**0.0611±0.0010**	**0.2041±0.0026**	**0.0997±0.0013**	**0.840±0.019**	**0.0311±0.0006**	**95**	**613±8**
7-1	**417**	**255**	**0.61**	**0.003**	**0.0602±0.0011**	**0.1857±0.0027**	**0.1007±0.0013**	**0.836±0.019**	**0.0306±0.0006**	**101**	**618±8**
8-1	78	40	0.51	0.006	0.0542±0.0030	0.1515±0.0072	0.0977±0.0014	0.730±0.042	0.0292±0.0015	159	601±8
9-1	**272**	**131**	**0.48**	**0.001**	**0.0592±0.0014**	**0.1433±0.0033**	**0.1005±0.0013**	**0.820±0.023**	**0.0299±0.0008**	**108**	**617±8**
10-1	**47**	**26**	**0.54**	**−0.004**	**0.0671±0.0049**	**0.1829±0.0117**	**0.0996±0.0015**	**0.922±0.070**	**0.0335±0.0022**	**73**	**612±9**
11-1	2135	759	0.36	0.018	0.0569±0.0011	0.1112±0.0026	0.0537±0.0007	0.422±0.010	0.0168±0.0004	69	337±4
12-1	**313**	**96**	**0.31**	**0.324**	**0.0806±0.0144**	**0.1852±0.0334**	**0.1106±0.0022**	**1.228±0.223**	**0.0665±0.0121**	**56**	**676±13**
13-1	**263**	**101**	**0.39**	**0.002**	**0.0587±0.0013**	**0.1111±0.0031**	**0.1013±0.0013**	**0.821±0.023**	**0.0292±0.0009**	**112**	**622±8**
14-1	*684*	*911*	*1.33*	*0.023*	*0.0610±0.0017*	*0.4104±0.0043*	*0.0984±0.0013*	*0.827±0.026*	*0.0303±0.0005*	*95*	*605±8*
15-1	*88*	*116*	*1.32*	*0.001*	*0.0611±0.0029*	*0.4238±0.0089*	*0.0975±0.0014*	*0.822±0.042*	*0.0313±0.0008*	*93*	*600±8*
16-1	**293**	**330**	**1.13**	**0.001**	**0.0604±0.0016**	**0.3421±0.0046**	**0.1013±0.0013**	**0.844±0.027**	**0.0308±0.0006**	**100**	**622±8**
16-2	1497	609	0.41	0.016	0.0581±0.0012	0.1239±0.0028	0.0638±0.0008	0.511±0.014	0.0194±0.0005	75	399±5
17-1	**105**	**70**	**0.67**	**0.019**	**0.0605±0.0049**	**0.2017±0.0117**	**0.0994±0.0014**	**0.829±0.070**	**0.0302±0.0018**	**98**	**611±8**
18-1	**94**	**65**	**0.70**	**0.002**	**0.0610±0.0036**	**0.2023±0.0089**	**0.1051±0.0015**	**0.884±0.056**	**0.0305±0.0015**	**101**	**644±9**
19-1	**277**	**339**	**1.22**	**0.001**	**0.0601±0.0009**	**0.3676±0.0036**	**0.1036±0.0014**	**0.859±0.019**	**0.0312±0.0005**	**105**	**636±8**
19-2	*768*	*77*	*0.10*	*0.001*	*0.0606±0.0007*	*0.0310±0.0014*	*0.0939±0.0012*	*0.785±0.015*	*0.0291±0.0014*	*92*	*579±7*
20-1	**117**	**112**	**0.96**	**0.002**	**0.0589±0.0023**	**0.2940±0.0064**	**0.1016±0.0014**	**0.826±0.036**	**0.0312±0.0008**	**111**	**624±8**
21-1	**177**	**197**	**1.12**	**0.003**	**0.0582±0.0020**	**0.3280±0.0055**	**0.1034±0.0014**	**0.830±0.032**	**0.0304±0.0007**	**118**	**635±8**
21-2	*563*	*192*	*0.34*	*0.003*	*0.0602±0.0010*	*0.1101±0.0023*	*0.0968±0.0013*	*0.804±0.018*	*0.0312±0.0008*	*97*	*596±7*
22-1	**81**	**53**	**0.65**	**0.004**	**0.0575±0.0050**	**0.1926±0.0119**	**0.1079±0.0016**	**0.856±0.077**	**0.0321±0.0021**	**129**	**661±9**
23-1	*324*	*76*	*0.24*	*0.002*	*0.0582±0.0010*	*0.0702±0.0023*	*0.0993±0.0013*	*0.797±0.019*	*0.0295±0.0011*	*114*	*611±8*
24-1	**79**	**78**	**1.00**	**0.000**	**0.0617±0.0012**	**0.2991±0.0048**	**0.1077±0.0015**	**0.916±0.023**	**0.0323±0.0007**	**100**	**660±9**
25-1	**96**	**42**	**0.44**	**−0.002**	**0.0613±0.0029**	**0.1313±0.0068**	**0.0968±0.0013**	**0.818±0.042**	**0.0291±0.0016**	**92**	**596±8**
25-2	*692*	*45*	*0.07*	*0.001*	*0.0607±0.0005*	*0.0195±0.0009*	*0.0985±0.0013*	*0.825±0.014*	*0.0295±0.0014*	*96*	*606±8*
26-1	**177**	**317**	**1.80**	**−0.002**	**0.0620±0.0018**	**0.5536±0.0063**	**0.0989±0.0013**	**0.846±0.029**	**0.0305±0.0006**	**90**	**608±8**
27-1	351	244	0.69	0.001	0.0586±0.0010	0.2085±0.0027	0.1004±0.0013	0.812±0.018	0.0301±0.0006	112	617±8
28-1	194	179	0.93	0.003	0.0581±0.0017	0.2758±0.0047	0.0991±0.0013	0.794±0.027	0.0295±0.0007	114	609±8
29-1	277	142	0.51	0.001	0.0624±0.0015	0.1564±0.0035	0.1033±0.0014	0.889±0.025	0.0316±0.0009	92	634±8
30-1	**689**	**289**	**0.42**	**0.000**	**0.0605±0.0005**	**0.1243±0.0013**	**0.1010±0.0013**	**0.843±0.014**	**0.0299±0.0005**	**100**	**621±8**
30-2	**374**	**187**	**0.50**	**0.000**	**0.0614±0.0015**	**0.1561±0.0037**	**0.0995±0.0013**	**0.843±0.025**	**0.0310±0.0009**	**93**	**612±8**
31-1	688	325	0.47	0.000	0.0607±0.0005	0.1402±0.0014	0.1049±0.0014	0.878±0.015	0.0312±0.0005	102	643±8
32-1	**248**	**125**	**0.50**	**0.000**	**0.0611±0.0008**	**0.1544±0.0021**	**0.1000±0.0013**	**0.843±0.017**	**0.0306±0.0006**	**95**	**614±8**

(UWA Mount 96-42 A).

f ^{206}Pb is the proportion of common Pb in ^{206}Pb, determined using the measured ^{206}Pb/^{208}Pb and Th/U ratios.

%conc. is concordance, as $100\{t[^{206}Pb/^{238}U]/t[^{207}Pb/^{206}Pb]\}$. Bold=cores, Italics=rims, Regular=homogeneous crystal.
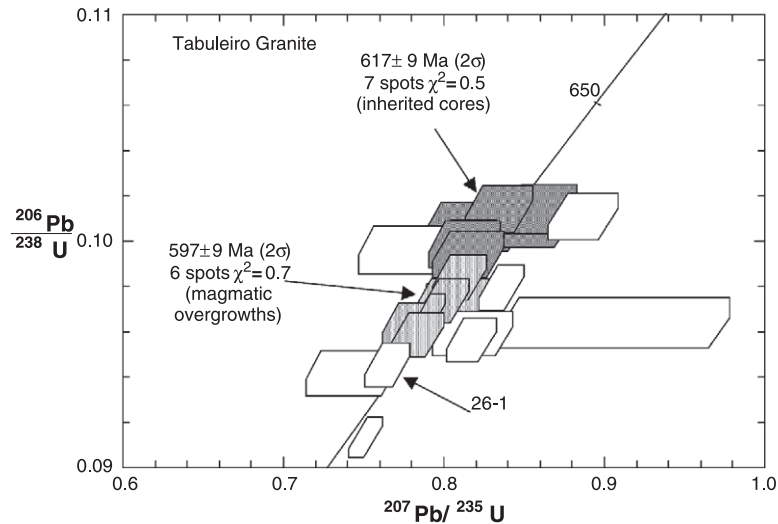
Fig. 6. Concordia plot for zircon data from sample 1 (Tabuleiro Granite). Discussion of the results and explanations for the discarded analyses (blank error boxes) are in the text. Age uncertainties at 95% confidence level for pooled analyses. Error boxes are 1σ.

nature (χ^2=1.1), and yield an age of 628±7 Ma (dark gray error boxes, Fig. 8).

3.1.3. Speculations on the sources of inherited zircon

Both analysed plutons are very homogeneous, allochthonous intrusion, with ca. 620–630 Ma inherited zircon populations. These ages are within the error for the age of syn-tectonic granitoids from the batholith, exposed in other segments of the batholith (ca. 625 Ma, Silva et al., 2003). Accordingly, short-lived syn-tectonic granitoids, rapidly recycled (re-melted) in low crustal levels, are likely source of Tabuleiro and Guabiruba inherited zircons. A crustal derivation of these magmas, is consistent with their chemical (A_2-type, sensu Eby, 1992 and I-Caledonian, sensu Pitcher, 1983) and Nd isotopic signatures (Silva, 1999).

4. Reassesment of U–Pb SHRIMP data from the banded anatectic granitoids from the Florianópolis Batholith (S3 and S4)

4.1. Geological setting

We also reassessed the U–Pb SHRIMP data and SEM images from two late-tectonic, banded anatectic granites previously studied by Silva et al. (2000) and

assigned to the Camboriú and Águas Mornas complexes. They consist of orthomigmatitic associations in which polyphasic (Paleoproterozoic) tonalitic gneisses (G_1) and amphibolites have been variably, but generally strongly, modified by Brasiliano-aged partial melting, assimilation and synchronous deformation (Figs. 3, 4 and 12). The melts, locally migrated from their sources (paleosomes), have formed veins, pockets, and larger intrusive granitic bodies of regional extent. In the sampled site they gave rise to strongly banded in situ *syn-tectonic* anatectic leucosomes (G_2, Figs. 3, 4 and 12). The major structural feature of the G_2 phase is a low angle gneissic subsolidus magmatic fabric (flow banding). Highly transposed thrust sheets are observed locally, and indicate syn-tectonic injection of granitic melt during a contractional tectonic phase.

4.2. Previous U–Pb data

An anatectic granitoid phase of the Camboriú Complex (correlated to S3) was dated by means of zircon ID-TIMS procedure (Babinski et al., 1997). It furnished a chord with an upper intercept apparent age of ca. 2730 Ma, and a lower intercept apparent age of ca. 550 Ma. The authors also obtained a Sm–Nd T_{DM} model age of ca. 2.16 Ga with a strongly negative ε_{Nd} value (-22) for t=0.6 Ga. Hence, the authors favoured
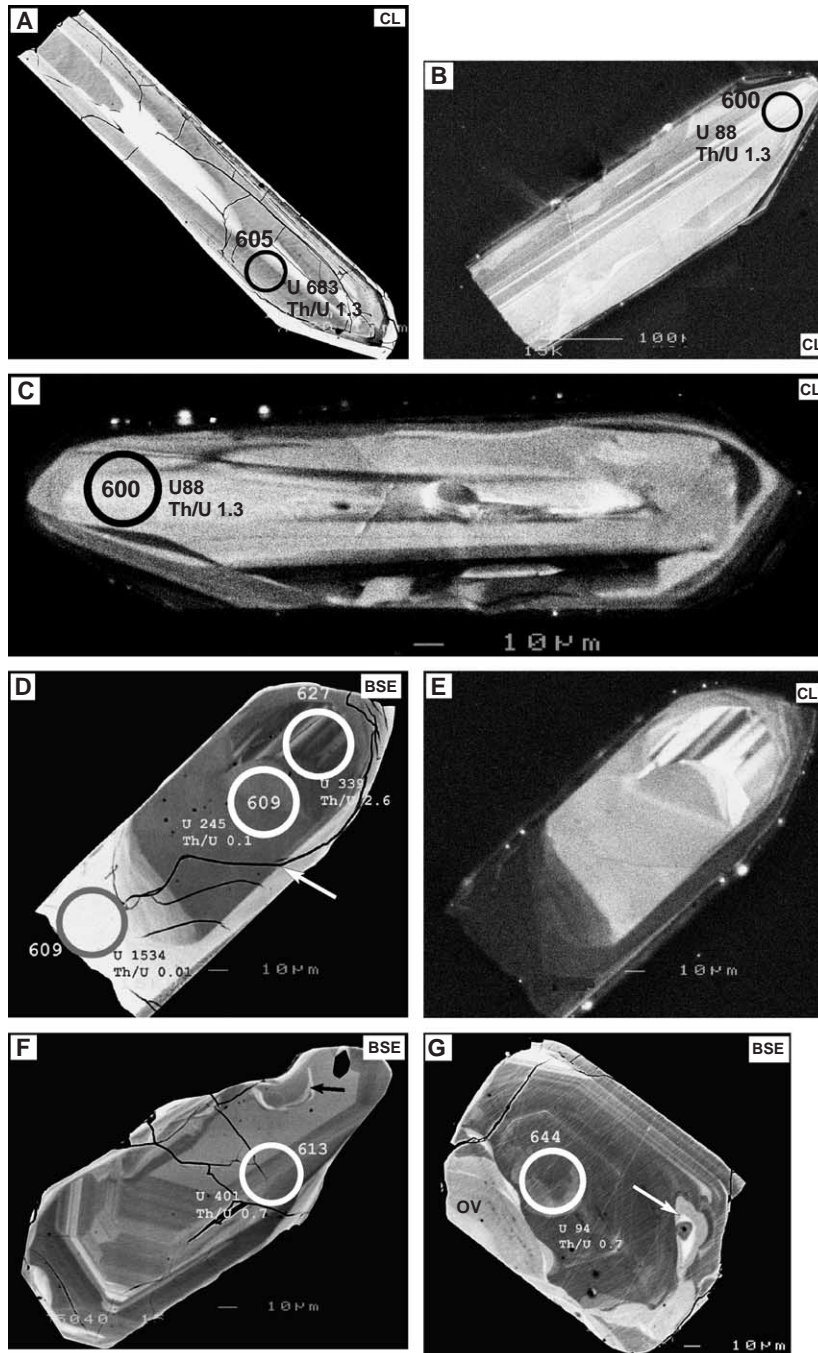
Fig. 7. Backscattered electron (BSE) and cathodoluminescence (CL) images of zircons from the sample 2 (Guabiruba Granite). Crystals numbering follows Table 2. (A) Crystal 5; (B) Crystal 15; (C) Crystal 17; (D–E)=Crystal 4. Arrow=expansion fractures; (F) Crystal 6; (G) Crystal 18 ov=scalloped (resorption) melt-precipitated overgrowth on inherited magmatic core (also displaying a halo around mineral inclusion). Circles (~ 30 μm)=SHRIMP spot location. Ages indicated in Ma; U in ppm.
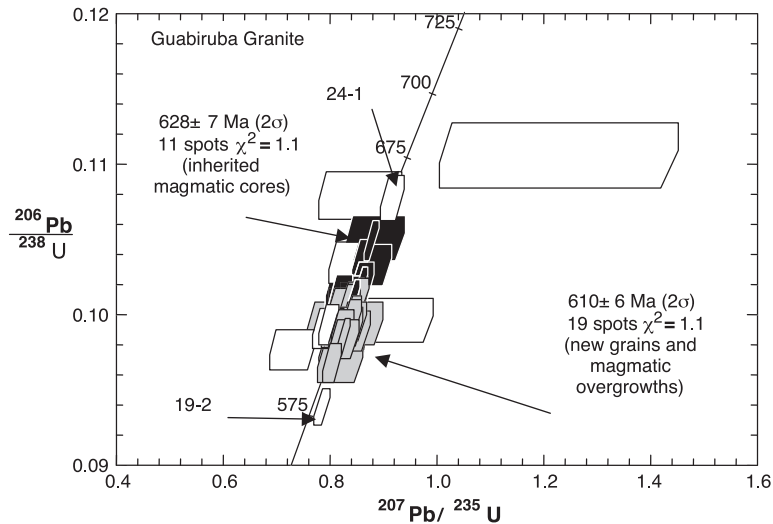
Fig. 8. Concordia plot for zircon data from Sample 2 (Guabiruba Granite). Discussion of the results and explanations for the discarded analyses (blank error boxes) are in the text. Age uncertainties at 95% confidence level for pooled analyses. Error boxes are 1σ.

an Archean/Paleoproterozoic crystallisation age and a Neoproterozoic overprinting for the banded anatectic granitoid.

Silva et al. (2000), by means of U–Pb SHRIMP systematics, dated the same banded anatectic granitoid from the Camboriú Complex studied by Babinski (S3-G$_2$, Figs. 3 and 4), and a similar anatectic gneiss from the Águas Mornas Complex (S4-G$_2$, Fig. 12). Magmatic textured inherited zircons cores in both samples provide highly concordant Paleoproterozoic apparent ages (upper intercept) of ca. 2000 Ma and ca. 2175 Ma, respectively. The Paleoproterozoic results were interpreted as the crystallization ages of the rocks, whereas the lower intercepts furnished apparent ages of ~ca. 600 Ma (S3) and 592±5 Ma (S4) and were interpreted as the age of metamorphic (solid-state) reworking of the Paleoproterozoic rocks. The same evolution was also previously favoured in the works of Babinski et al. (1997) and Hartmann et al. (2000).

Basei (2000) dated other foliated anatectic granite from the Camboriú Complex by ID-TIMS zircon U–Pb systematics, and proposed an alternative inter-

pretation. The analytical results form a discordant array with a lower intercept apparent age of 583±23 Ma, interpreted as the crystallization age, and an (imprecise) upper intercept apparent age of ca. 2800 Ma (cf. Babinski et al., 1997) interpreted as inherited age. Silva et al. (2002) analyzed rocks from the same outcrop, using zircon SHRIMP systematics and obtained an age of 2174±22 Ma for the cores, and an imprecise 860±330 Ma age for the rims. The authors favoured an interpretation of Paleoproterozoic crystallization age, but also considered that the rims could also been derived from Neoproterozoic melt-precipitated new zircon, and the cores represent inheritance, in agreement with Basei (2000).

We explore these interpretative contradictions by re-examining a larger database of BSE and CL imaging from S3 and S4 (Figs. 9 and 13; in Fig. 2). The U–Th–Pb isotopic data tables, chemical and petrographic descriptions, methodology, and the other SEM images can be found in the (Silva et al., 2000) paper, but the concordia diagrams (Figs. 11 and 14) are reproduced here from Silva et al. (2000) to clarify the new interpretation of the data.

Fig. 9. Backscattered electron (BSE) and cathodoluminescence (CL) images of zircons from sample 3 (G$_2$ Banded anatectic syenogranite/Camboriú Complex). Grains numbering follows Table 1 (Silva et al., 2000). (A–B) Crystal 23; (C–D) Crystal 6; (E–F) Crystal 3; (G–H) Crystal 7. "rs"=resorption inner rim, located between the inherited cores and rims and "sf"=sealed fracture. Circles (~30 μm)=SHRIMP spot location. Ages indicated in Ma.
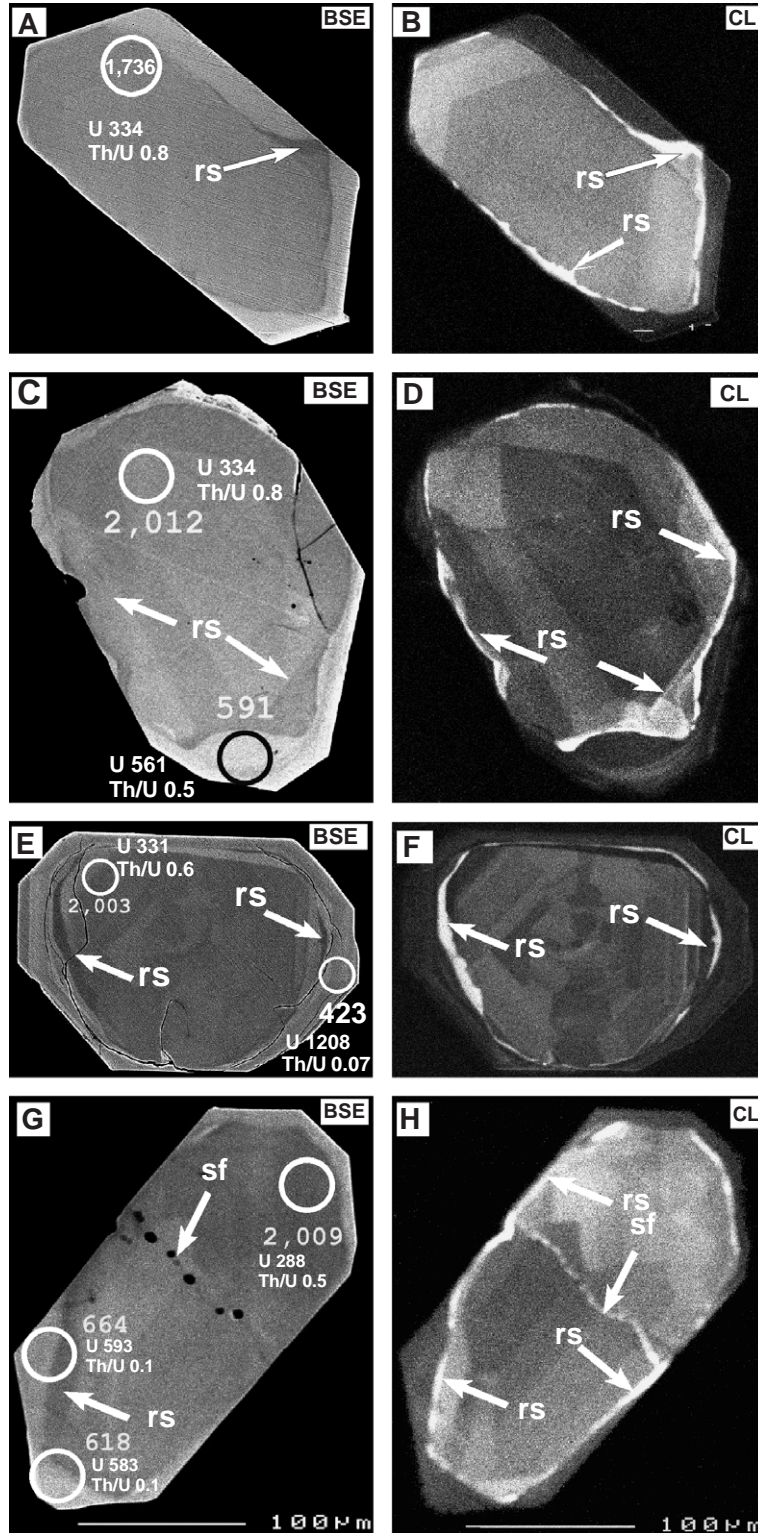
4.3. Zircon morphology, and U–Th–Pb data re-interpretation

The new BSE/CL imagery from S3 and S4 zircons is characterized by euhedral crystals, mostly with prismatic habit showing internal sharp discrimination between inherited core and the rim (Figs. 9 and 13). Cores are volumetrically dominant, forming up to 95% of some crystals in both samples. S3 shows unimodal distribution of magmatic-textured inherited ca. 2000 Ma cores, whereas S4 shows a wide distribution of magmatic and metamorphic core ages, from ca. 2900 Ma to ca. 620 Ma (Subgroups 2.1–2.3). Magmatic cores typically lack oscillatory zoning in BSE and CL images, but sector zoning characteristic of magmatic growth (e.g. Hanchar and Miller, 1993) is ubiquitous in the CL images (Figs. 9B,D,F,H and 13B,F,G). The magmatic cores are medium grey in both BSE and CL images, containing ca. 200–300 ppm U and low Th/U, which permits their discrimination from the metamorphic core subgroups, which show U- and Th-depletion and Th/U ratios >0.8, higher than expected for typically metamorphosed zircons.

As compared with zircons from S1 and S2, the internal morphology of S3 and S4 is much more complex. Most crystals are characterized by three successive shells: an inherited core, a thin (<5 μm) U-poor, high luminescent in CL, inner resorption rim, and a larger, melt-precipitated euhedral outer rim (details in Fig. 10).

The outer rims are only a few micrometers (<5 μm) wide in some crystals, but may reach 50 μm or more. The average width is estimated at 10 μm but exhibits considerable variation even in a single crystal. Volumes of rims vary between 10% and 20% of the crystal. The rims are grey to bright in BSE, and dark in CL, showing irregular, sometimes curvilinear smooth contacts with the (resorbed) cores, but on the whole they have an outermost euhedral, prismatic form (Fig. 9A,E,G). Most rims also show well-defined fine-scale oscillatory-zoned textures, typical of magmatic crystallization (S3, Fig. 9C–D, E–F) (S4, Fig. 13A–J).

In most crystals, a narrow (<5 μm), discontinuous, curvilinear inner zircon rim occurs between the inherited core and the outer rim overgrowth. These inner rims, which are dark in BSE and bright in CL,
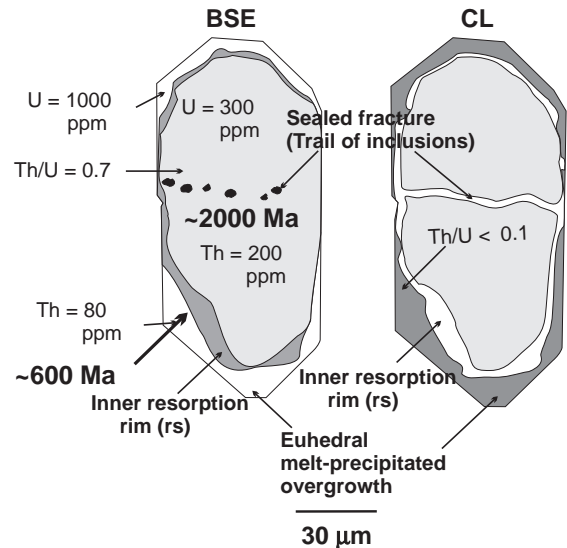
Fig. 10. Sketch model of zircon zonations, based on Crystal 7 (Fig. 7 C–D) from sample 3 (G₂ Banded anatectic syenogranite/Camboriú Complex), illustrating the polyphase evolution deduced from the BSE/CL images and the U–Th distribution, from SHRIMP determinations. "rs"=resorption inner rims, located between the inherited cores (not to scale) and rims and "sf"=sealed fracture. (modified from Silva et al., 2000).

cut across the internal growth banding of the over-grown core ("rs" in Figs. 9 and 13E–F and G, S4). This zircon phase is typically U-poor as indicated by their high luminescence in CL images. Vavra et al. (1996) observed similar internal relationships in zircons from a polyphase, partially melted ortho-granulite, and described the U-depleted rim as a resorption-induced recrystallization seam, or resorption on surface with recrystallization seams ("rs"). The position of the bright (in CL) inner recrystallization rim ("rs"), between the discretely resorbed magmatic core and the dark (in CL) overgrowth, is interpreted as a continuum of chemical modifications at a "moving front", preceding the advancing resorption, and hence, a recrystallized domain from the original magmatic core, probably under solid-state conditions. For the development of the external euhedral rims overgrowth the main forming mechanism is attributable to anatectic melting-precipitation of new zircon material (overgrowths). An anatectic origin for the overall process as proposed by Vavra et al. (1996) is also favoured in the present study, but distinctly of what was noted in the zircons studied by Vavra et al. (1996), in our samples the resorption rims do not

represent the final stage of the morphologic evolution of the crystals as they are overgrown by melt-precipitate new zircon outer rims (Figs. 9 and 13). Fig. 10 depicts the intricate internal morphology of the zircon population illustrated by crystal #7 (Fig. 9G–H). The unaltered magmatic core is medium gray tones in both BSE and CL images, whereas internal rims ("rs") are dark gray in BSE and complementary bright in CL images (low-U contents). Inclusions along fractures are sealed by new zircon material that is dark (BSE) and bright in CL, owing to low U-contents.

Another kind of thin inner rim, bright in BSE and dark in CL ("mt" in Fig. 13 E–F, and H-S4) occurs immediately below the core/rim boundary, appears to be corroding the external parts of the core and locally protruding into the overgrowth (arrow in G–H). Similar bands were described by Vavra et al. (1996). The authors described similar bands as mantles of reduced CL intensity and interpreted them as segregation of impurities components extracted from the recrystallized parts of the core, during the anatectic process.

In addition to the melt-precipitated nature of the zircons overgrowths deduced by the SEM studies, the measurements of isotopic compositions of cores and rims yield additional significant information about the petrological events recorded within the cores and rims. The U concentration is ca. 300 ppm in magmatic cores and up to ca. 400–1200 ppm in melt-precipitated rims, whereas Th contents from cores and rims are in the 50–250 ppm range. Thus, the Th/U ratios from both magmatic-textured core and rim populations range from 0.1 to 1.0 as generally observed in magmatic zircon from felsic anatectic melts, but for the U-enriched magmatic rims (Figs. 9E and 13C,E,G), the Th/U ratios are lower than 0.1, owing to the anomalous enrichment in U.

The synthesis of morphological and isotopic evolution of the zircon populations are illustrated in the sketch model of the Fig. 10.

4.3.1. $^{206}Pb/^{238}U$ and $^{207}Pb/^{206}Pb$ ages from Camboriú Complex anatectic granite (S3)

Fourty-five analyses were performed on 34 zircons (Silva et al., 2000) from two distinct morphological groups. Group 1 analyses were performed on melt-precipitated overgrowths and on discrete new mag-

matic crystals (Fig. 11, Table 2) Owing to the very thin width of the rims the SHRIMP analysis area was wholly on the rim in only a few cases as spot #6-2 (Fig. 9C), which sputtered only the rim and yielded an age of 591±6 Ma. This apparent age, as well as the ages obtained on spots #9-1 and #9-4 (591±6 Ma and 581±5 Ma, respectively) are younger than the age of the G_3 granite (S2), which cuts the analysed sample and cannot be used as approximate crystallisation ages. Other analyses sputtered mixed core/rim material in various proportions, resulting in meaningless apparent ages likely ca. 664 Ma and 618 Ma (Fig. 9 C). Additionally, radiation damage due to high U-contents (>1000 ppm), which caused locally open-system isotopic behavior (Pb-loss), altered the original $^{206}Pb/^{238}U$ ratios of some overgrowths domains. Much younger ages of 203±2 Ma (spot #13-2 and #11-2) and 423±4 Ma (spot #3-2) are attributed to modern Pb-loss. Accordingly, results are scattered along concordia diagram between 203 Ma and 664 Ma and do not form a single coherent population that would justify pooling the $^{206}Pb/^{238}U$ data. Accordingly, the geological reliability of the data obtained on the larger core population (Fig. 11) is much higher. The 610±6 Ma crystallisation age of the G_3 granite (S2), which cuts the anatectic flow foliation of the analyzed rock (Figs. 2 and 3), provides a better constrained minimum age ≥610±6 Ma for the migmatitic event, approximation that is also supported by another migmatitic granite at the southern tip of the Orogen (Pinheiro Machado Complex), which yielded similar age of 609±7 Ma (Silva, 1999).

Analyses from inherited magmatic cores comprise 25 concordant analytical spots, forming a single cluster with little excess scatter of geological origin (χ^2=1.08), that yielded an age of 2006±3 Ma (Dark grey error box in Fig. 11 and inset, Table 2). The highly concordant $^{207}Pb/^{206}Pb$ ratios (mostly 95–99%) are remarkable results in terms of reliability of age determinations for an inherited core population that has survived an advanced partial melting process. They are strong evidences that the inherited Paleo-proterozoic cores remained isotopically closed during the crystallisation of the anatectic magma G_2 at ca. 610 Ma (the age of the melt-precipitated overgrowths) and represent well-preserved melt restitic source material, dominantly composed of a single Paleoproterozoic source. The adjacent tonalitic country rock is
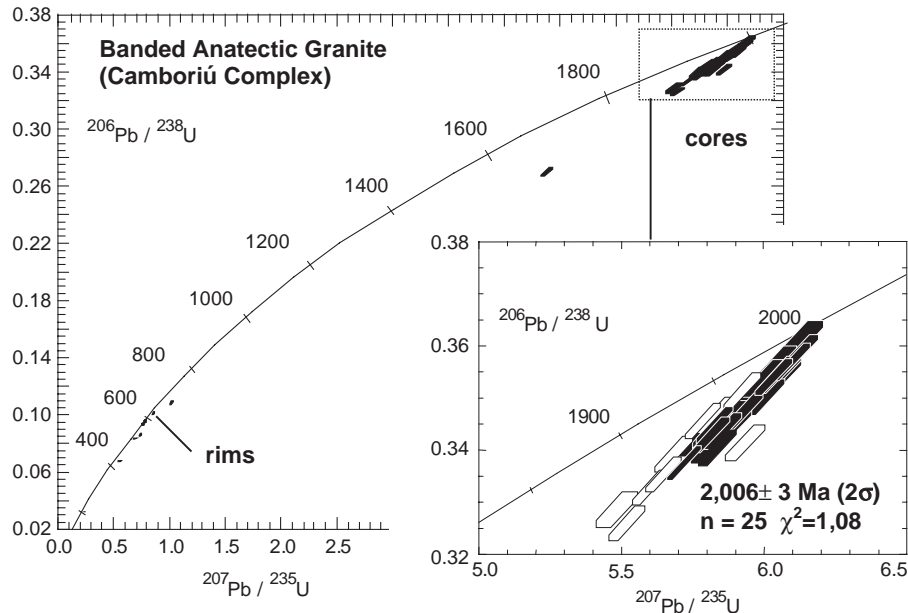
Fig. 11. Concordia plot for zircon data for Sample 3 (G$_2$ Banded anatectic syenogranite/Camboriú Complex). Inset shows details of the main population (Group 1). Discussion of the results and explanations for the discarded analyses (blank error boxes) are in the text. Age uncertainties at 95% confidence level for pooled analyses. Error boxes are 1σ.

the most probable source (paleosome) which supplied the melt with the large ca. 2000 Ma zircon inherited population. The excellent correlation of U and Th magmatic contents of the 2000 Ma-old cores (Silva et al., 2000) confirms that they were restitic component unaffected, or little affected, by the process that generated the rims (melt-precipitation) (Fig. 12).

4.3.2. $^{206}Pb/^{238}U$ and $^{207}Pb/^{206}Pb$ ages from Águas Mornas Complex anatectic granite (S4)

Forty-five analyses were performed on 34 zircons (Silva et al., 2000) from two distinct morphological groups. Group 1 analyses (Fig. 14) from magmatically-textured rims and homogeneous new crystals form a single morphologically uniform cluster (n=5), with no detectable scatter of geological origin (χ^2=0.40), with $^{206}Pb/^{238}U$ age of 592±5 Ma (grey error boxes, inset A). The result is interpreted as the crystallization age of the anatectic granodiorite. Data from several spots with discordant results (>10%), high U-content (>1100 ppm), or data from mixed core/rim domains, are not considered.

Group 2 analyses comprise several populations of magmatic and metamorphic inherited cores and

xenocrysts. The main pooled core population consists of Paleoproterozoic cores (e.g. Fig. 13A–B). They form a single morphologically uniform group (n=9), without apparent scatter of geological origin (χ^2=0.46), yielding a $^{207}Pb/^{206}Pb$ age of 2175±13 Ma (Fig. 14, inset B). The data are interpreted as the age of a zircon population derived from the partially melted country-rock. The preserved magmatic domain of the highly complex inherited core of crystal #21 (Fig. 13G), yields a younger concordant crystallization age of 1985±13 Ma (1σ), and hence it could represent a younger paleosomatic source or slight Pb-loss from older zircon. Another result obtained on a discrete homogeneous crystal, morphologically resembling the main magmatic core population (spot #3.1), was also discarded owing to its older crystallization age of 2234±18 Ma (1σ) probably representing zircon from an older granitic paleosomatic source. The significance of these two concordant results in the context of the regional evolution was not clarified in the present study, as there are no exposed rocks units with these ages in the region.

Subgroup 2.1 is formed by 3 concordant inherited high luminescente (CL) cores with low-U contents,
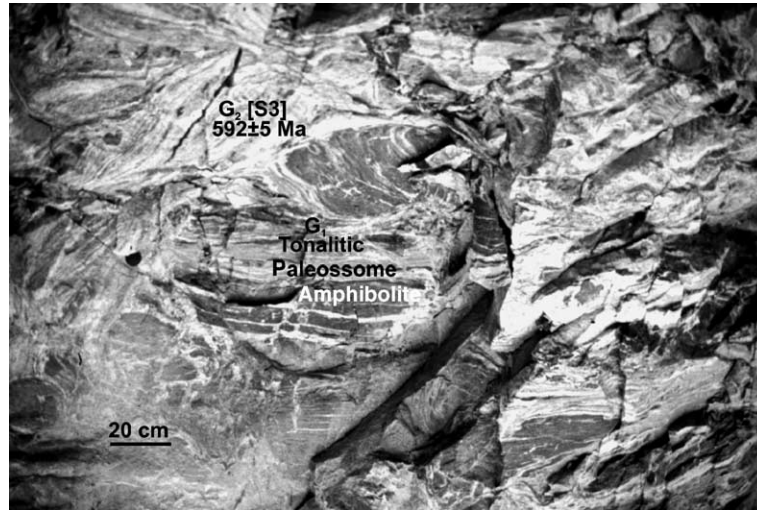
Fig. 12. Polyphase migmatitic gneiss from Águas Mornas Complex (Banded anatectic monzogranite) at S4 sample site (BR-470 highway, vicinities of Águas Mornas town), featuring cross-cutting intrusive relations of dated G_2 late-tectonic banded anatectic gneiss (light gray). The complex folded G_1 tonalitic remnants (medium gray paleosome) show abundant concordant (in situ) and injected leucosome bands and pockets (white). Note the presence of a well-preserved amphibolite bands discretely injected by G2. Polyphase migmatitic gneiss from Camboriú Complex at S3 and S4 sample site.

typical of high-grade metamorphic overprinting, with apparent ages ranging from ca. 2191 Ma to ca. 2150 Ma. Spot #18-1 (Figs. 14, inset B, 13H) furnished a metamophic apparent age of ca. 2191±17 Ma, with unknown regional significance. The concordant apparent ca. 2150 Ma $^{207}Pb/^{206}Pb$ ages, respectively from crystals #17 and #22, may be related to a younger metamorphic episode locally affecting the ca. 2175±13 Ma main pooled magmatic core population, or fortuitous coincident due to Pb-loss.

Subgroup 2.2 comprises 3 concordant inherited high luminescente (CL), low-U cores (crystals 22 and 23) with metamorphic apparent ages of ca. 1750 Ma, (Fig. 14, inset C). The former (crystal #22) furnished metamorphic $^{207}Pb/^{206}Pb$ ages of 1744±22 Ma and 1757±38 Ma (1σ). The latter (crystal #23 Fig. 13I–J), yielded a metamorphic $^{207}Pb/^{206}Pb$ apparent age of ca. 1736±17 Ma (1σ). This subgroup of ca. 1750 Ma is interpreted as the age of a high-grade metamorphic event that could have affected the anatectic granitic source, previously to its remelting at ca. 600 Ma. Hence, it is a second indirect isotopic indication of late Paleoproterozoic (Satherian) record in the region; the first record was suggested by the presence detrital zircons of ca. 1750 Ma (Silva et al., 2002), found in Neoproter-

ozoic felsic tuffs, exposed some 100 km N of S4 exposure. In this subgroup, another high-grade, annealed rounded core, yielded much younger metamorphic ages of 618±6 Ma (1σ) and 613±5 Ma (1σ) (respectively, spots #14-1 and #14-2, Fig. 13C–D). These low-U, annealed, rounded (globular) cores may be interpreted as products of multiple episodes of metamorphic growth (e.g. Hanchar and Miller, 1993), which underwent total erasing of their isotopic memory previous to its recrystallization (e.g. Friend and Kinny, 1995), at ca. 615 Ma. On the other hand, this apparent 615 Ma metamorphic age matches the syn-tectonic metamorphic peak (630 and 610 Ma) recorded in other segments of the arc. Hence, it represents an older, probably, detrital zircon population, which experienced high-grade metamorpic conditions at ca. 615 Ma, immediately before the partial melting event, responsible for the crystallisation of its new zircon rim, dated at ca. 581±4 Ma (Fig. 13C).

Subgroup 2.3 comprises two crystals with Archean highly concordant magmatic ages. Analysis spot #15 (Fig. 13E–F) yielded a cyrstalization age of 2707±7 Ma (1σ), whereas spot #20 furnished a crystallization age of 2934±3 Ma (1σ). The regional geological significance of these magmatic apparent Archean ages
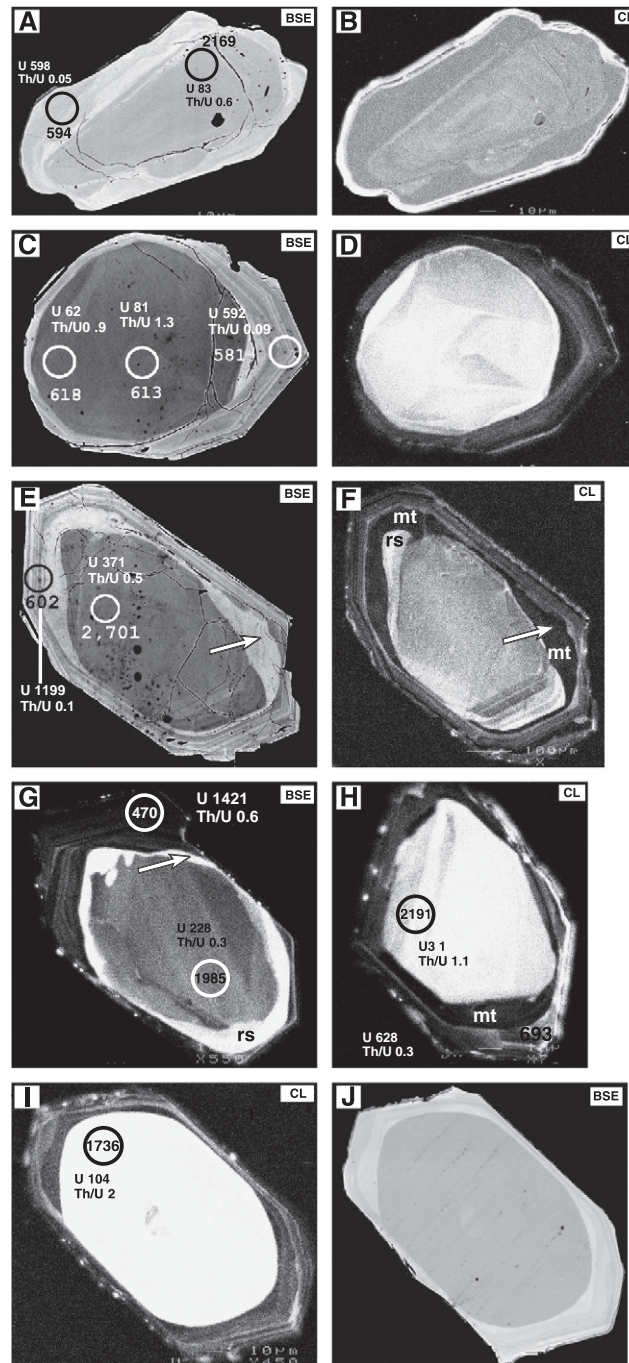
Fig. 13. Backscattered electron (BSE) and cathodoluminescence (CL) images of zircons from sample 4 (G$_2$ Banded Anatectic monzogranite/ Águas Mornas Complex). Crystal numeration follows Table 3 (Silva et al., 2000). (A–B) Crystal 13; (C–D) Crystal 14; (E–F) Crystal 15; (G) Crystal 21; (H) Crystal 18, (I–J) Crystal 23; "rs"=resorption inner rims; and "mt"=mantle of reduced CL intensity, both located between the inherited cores and rims. Circles (~30 μm)=SHRIMP spot location. Ages indicated in Ma; U in ppm.
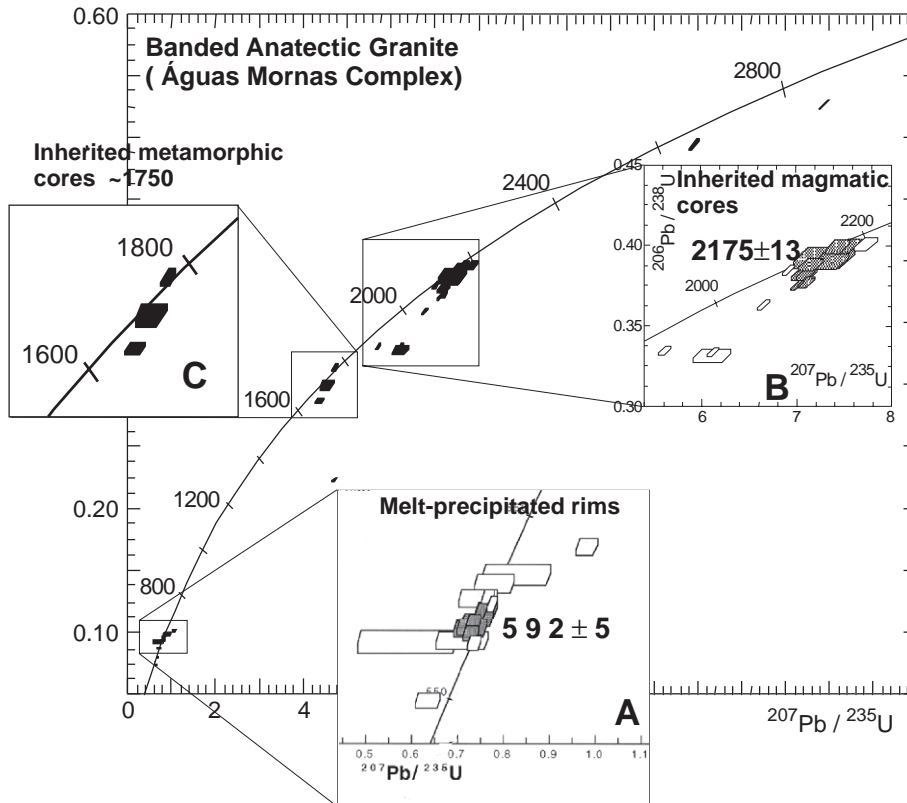
Fig. 14. Concordia plot for zircon data from sample 3 (G$_2$ Banded anatectic monzogranite/Águas Mornas Complex). Inset A: details of overgrowths main population (Group 1). Inset B: detail of the spreading of ages, close to 1600 Ma. Inset C: detail of the main pooled cluster of inherited core (Group 2). Discussion of the results and explanations for the discarded analyses (blank error boxes) are in the text. Age uncertainties at 95% confidence level for pooled analyses. Error boxes are 1σ.

is unknown, but the basement of the orogen, exposed some 150 km N of the studied area, is composed of an Archean TTG gneisic complex, dated at ca. 2700 Ma.

5. Discussion and conclusions

This investigation is also a case study on the growing importance of spatially-resolved U–Pb SHRIMP systematics, preceded by SEM imaging, to arrive at better interpretations populations with multiple episodes of zircon evolution. The interpretations benefit from comparisons of zircons with similar internal morphology, well characterized in other crustal-derived granitoids elsewhere (e.g. Williams, 1998) and on polyphase gneissic migmatitic rocks (Hanchar and Miller, 1993; Vavra et al., 1996, 1999, among others). Table 3 summarizes the internal

features and correlates each textural domain to a particular petrologic process.

The internal morphological complexity reported above explains the distinct interpretation of the results obtained on sample 3 obtained by Babinski et al. (1997) by means of ID-TIMS and without the support of previous SEM imaging and even. Even using SHRIMP systematics, previous attempts to unravel the $^{206}Pb/^{238}U$ anatectic crystallization age was not successful (Silva et al., 2000; Hartmann et al., 2000), despite the large number of analytical spots (43) on 33 crystals. Owing to the study of a small number of SEM images the authors failed to fully recognize the magmatic (melt-precipitated) nature of the euhedral Neoproterozoic overgrowths and new crystals, which they interpreted as metamorphically-recrystallized Paleoproterozoic zircons. Additionally, the statistical bias caused by the overwhelming dominance of a

Table 3
Interpretation of zircon internal morphology and zonation patterns in BSE and CL images, and U–Pb ages of the 4 studied samples

Samples	Inherited cores		Overgrowth rims and new crystals	
	BSE/CL zonation patterns and interpretations	Pooled ages (Ma)	BSE/CL zonation patterns and interpretations	Pooled ages (Ma)
Sample 1 (Tabuleiro Granite)	1. Prismatic, gray tons; oscillatory zoned=magmatic. 2. Rounded, oscillatory zoned, with irregular external shape=resorbed magmatic. 3. New zircon sealed fractures and inclusions trails.	617±9	1. Outer, euhedral, oscillatory zoned, normal, to high-U (dark in CL)=final growth in melt.	597±0
Sample 2 (Guabiruba Granite)	Same as above.	628±17	Same as above	610±6
Sample 3 (G2 Anatectic syenogranite (Camboriú Complex)	1. Prismatic, gray tons; sector-zoned=magmatic. 2. Subrounded, medium gray (BSE and CL) rounded, sector-zoned=resorbed magmatic. 3. New zircon sealed fractures and inclusions trails.	2006±3	1. Outer euhedral, oscillatory zoned, high-U (dark in CL)= final growth in melt. 2. Inner, low-U (bright in CL) curvilinear, separating core from rim ("rs": resorption seams)=pre-anatexis.	Undetermined (>ca. 620–610 indirect Indication)
Sample 4 (G2 banded anatectic monzogranite (Águas Mornas Complex)	1. Subrounded, prismatic; oscillatory zoned, grey in BSE and CL=magmatic. 2. Rounded, oscillatory zoned, grey in BSE and CL=magmatic. with irregular external shape=resorbed magmatic. 3. Subrounded and prismatic, Low-U (gray in BSE and bright in CL), annealed=high-grade metamorphic.	2175±13	1. External euhedral, oscillatory zoned, high-U (dark in CL) and high-Th=final growth in melt. 2. Inner, low-U (bright in CL) curvilinear, separating core from rim ("rs": resorption seams)=pre-anatexis. 3. Inner, curvilinear, light gray in BSE, dark in CL, separating core from rim protruding the rim ("mt") mantle of reduced CL intensity=segregation of impurities, from the recrystallized portions, during anatexis.	592±5

much greater number of highly concordant, voluminous magmatic-textured cores population over thin, high-U discordant overgrowth rims, also explains this ambiguous interpretation.

The high U-contents of the melt-precipitated rims (up to 1200 ppm), with predictable susceptibility to Pb-loss compared to the lower U-content of the SHRIMP standards, explains part of the analytical problems on determining the precise crystallisation age of rims. Similar analytical and interpretative problems were also noticed in a preliminary analysis of the data from samples 1 and 2, with results remaining unpublished as part of a PhD thesis (Silva, 1999). Finally, the dispersion of concordant ages between ca. 2175 Ma

and ca. 600 Ma obtained on metamorphic inherited cores, with ages of ca. 2150 Ma, 1750 Ma and ca. 620 Ma is interpreted as due to variable Pb-loss during the ca. 600 Ma metamorphic overprinting of the original ca. 2175 Ma magmatic core population.

We have no information on the petrogenetic processes controlling the original contents of zirconium and its partitioning in the melted fraction, and hence we are not able to discuss the probable cause(s) of the preservation of such a large volume of inherited zircon, even under advanced partial melting. Williams (1998) ascribes the preservation of abundant inherited zircon phases in some S-type granitoids as due to crystallisation under relatively low temperatures.

The results confirm the well known property of zircon that causes its U–Th–Pb isotopic system to remain closed-system by domains, allowing the discrimination of older from younger events, whenever the young domains reached equilibrium, even for the studied populations which underwent advanced partial melting processes.

In addition to furnish new insights in the tectono-magmatic evolution of the Florianópolis Batholith, as far as the geology and granite chronostratigraphy of the studied area is concerned, the major consequence of the previous age interpretations was that the exposed area of Paleoproterozoic rocks was greatly overestimated in previous works. The entire region of granitic and migmatitic gneisses distributed along a belt of some 80 km long and U–Pb to 30 km wide ascribed to the Camboriú, Águas Mornas complexes (Fig. 2), has been mapped as a Paleoproterozoic unit (metamorphosed during the Neoproterozoic event). The present re-interpretation has clarified the polycyclic evolution of both complexes. Hence, and as the Paleoproterozoic country-rock do not define a continuously exposed unit, it is necessary to undertake a detailed re-examination of the field relations to discriminate cartographically between Paleo and Neoproterozoic components.

The new U–Pb isotopic study is consistent with the characterization of the batholithic magmatism as related to dominantly recycled, mature continental arc (Pelotas Arc in Fig. 1). Basei (1985), Mantovani et al. (1987); Babinski et al. (1997), Silva (1999) used chemical and Sm–Nd isotopic data to characterize remelted Paleoproterozoic/Archean lower crustal gneisses, recycled Neoproterozoic granitic material, with restrict juvenile additions, as the major sources for the Neoproterozoic granitoids.

Appendix A. Location and characterization of the post-tectonic granites (samples 1 and 2)

A.1. Tabuleiro Granite (S1)

Sample 1 was collected at the Cambirela quarry, 0.7 km south and 0.7 km west of the BR-101 highway bridge over the Rio do Matias (Fig. 2), exposed in the quarry are a rhyodacitic plug and associated pyroclastics. The sample was collected from a 10 m×10 m×10 m granitic block intruded by the rhyolite, showing very sharp contacts indicative of a shallow crustal level of intrusion of the granite.

The Tabuleiro Granite is a very homogeneous pluton, with sparse oval-shape autolithic enclaves. The quartz dioritic cognate igneous materials contain K-feldspar phenocrysts that are compositionally similar to those in the granitic matrix, suggesting magma-mingling processes. The sample is syenogranitic, leucocratic, medium- to coarse-grained, with equigranular subsolvus seriate or unmantled porphyritic texture. Quartz and mesopertithic feldspar are the main components. Biotite is the main accessory mineral, and minor accessories include zircon, allanite, topaz, opaque minerals, and fluorite. Alteration consists of fine-grained aggregates of chloritized and sericitized biotite and saussuritized plagioclase. Zircons are mainly included in former biotite (now chlorite) crystals; some zircon grains show a strong, pervasive metamictization.

Chemically, the sample presents an A_2-type chemical signature (sensu Eby, 1992) not modified by the intense post-magmatic alteration: high SiO_2 (71.1%), high alkalis (Na_2O+K_2O 8.4%) and low Al_2O_3 and CaO (14.2% and 2.3%), respectively. The A_2-type chemical signature suggests it originated by partial melting of metaluminous orthogneiss at deep crustal levels (e.g. Wahlen et al., 1987; Sheraton and Black, 1988). The ca. 1.7 Ga T_{DM} model age and the

(moderately) negative ε_{Nd} value (-4) is an additional evidence of a long-lived crustal source for the magma (Silva, 1999), implying a mixed-source model between Paleo/Meso and Neoproterozoic (inherited zircons) complex isotopic inheritance.

A.2. Guabiruba Granite (S2)

This granite (G_3, within the regional granitic stratigraphy) intrudes the Neoproterozoic syn-tectonic, banded anatectic phase (G_2, S3, see below). It occurs as a post-kinematic (post-tectonic) intrusion located at the northern limit of the Florianópolis Batholith, at the Caseca quarry, 3 km south of the BR/101 highway bridge over the Camboriú River (Figs. 2–4).

Petographically, S2 is a leuco-monzogranite with medium-grained seriate hypidiomorphic, isotropic texture. Sodic plagioclase, quartz and microcline are the essential minerals, chloritised biotite the main accessory, and allanite and zircon are minor accessories. Post-magmatic low-temperature alteration includes fine-grained saussuritization of the plagioclase, sericitization of the microcline, and muscovitization and chloritization of the biotite.

Chemically this rock has an HKCA signature: high SiO_2 (72.3%), high alkalis (Na_2O+K_2O 8.3%) and low Al_2O_3 and CaO (14.1% and 1.5%, respectively), corresponding to the I-Caledonian, crustal-derived post-tectonic granites (sensu Pitcher, 1983). The ca. 2.5 Ga T_{DM} model age and the (strong) negative ε_{Nd} value (-24) is an additional evidence of a long-lived crustal source for the magma (Silva, 1999), implying a mixed-source model between Archean and Neoproterozoic (inherited cores) complex isotopic inheritance.

Appendix B. SHRIMP methodology

B.1. Sample preparation

Approximately 10 kg of each rock sample was collected and processed by conventional methods, starting with crushing, milling and sieving. Heavy minerals in the 80–150 mesh fraction were concentrated by heavy liquids, followed by zircon separation by magnetic methods and hand picking.

About 100 crystals were collected from the least magnetic zircon fraction, and cast in a standard 2.5 cm epoxy mount and sectioned by polishing. The mount was initially carbon-coated for backscattered electron (BSE) and cathodoluminescence (CL) imaging using the JEOL 6400 scanning electron microscope (SEM) at the Centre for Microscopy and Microanalysis, University of Western Australia. BSE and CL images were made of all the crystals before performing SHRIMP analyses.

B.2. SHRIMP II procedures

The isotopic U–Pb analyses were obtained using the SHRIMP II at Curtin University of Technology in Perth, Western Australia. Instrumental conditions and data acquisition have been described in Compston et al. (1984, 1992). The SHRIMP operation and specific procedures followed the routine described by Smith et al. (1998). The analytical work was accomplished in four sessions of 24 h each. Pb, U and Th concentrations were referenced to the standard zircon (cz3). One determination on the standard was obtained for each three analyses on the unknown (ca. 30 μm diameter spot size). The age uncertainties are cited at the 95% confidence level for the selected populations, and the internal precision for single analyses in tables and figures is 1σ.

References

Babinski, M., Chemale Jr., F., Van Schmus, W.R., Hartmann, L.A., Silva, L.C. da, 1997. U–Pb and Sm–Nd geochronology of the Neoproterozoic granitic-gneissic Dom Feliciano Belt, southern Brazil. J. South Am. Earth Sci. 10, 263–274.

Basei, M.A.S., 1985. O Cinturão Dom Feliciano em Santa Catarina. (Dr. Thesis). IGC/USP São Paulo, 186 pp. (Unpublished).

Basei, M.A.S., 2000. Geologia e Modelagem geotectônica dos terrenos pré-cambrianos das regiões sul-oriental brasileira e uruguaia: possíveis correlações com províncias similares do sudoeste africano.(Livre Docência Thesis). IGC/USP, São Paulo, 123 pp. (Unpublished).

Chemale Jr., F., Malmman, G., Bitencourt, M.F., Kawashita, K., 2003. Isotope geochronology of syn-tectonic magmatism along the Major Gercino Shear-Zone: implications for the timing of deformation events. 4th South America symposium on isotope geology. Salvador, 2003. Short papers, pp. 516–519.

Compston, W., Williams, I.S., Meyer, C., 1984. Geochronology of zircons from the lunar breccia 73217 using a sensitive high mass resolution ion microprobe. J. Geophys. Res. 89 (Supp. B), 525–534.

Compston, W., Williams, I.S., Kirschvink, J.L., Zichao, Zh., Guogan, M., 1992. Zircon ages for the Early Cambrian time-scale. J. Geol. Soc. (Lond.) 149, 171–184.

Eby, G.N., 1992. Chemical subdivision of A-type granitoids: petrogenetic and tectonic implications. Geology 20, 641–644.

Friend, C.R.L., Kinny, P.D., 1995. New evidence for protolith ages of Lewisian granulites, northwest Scotland. Geology 11, 1027–1030.

Gebauer, D., Schertl, H.-P., Brix, M., Schreyer, W., 1997. 35 Ma old ultrahigh-pressure metamorphism and evidence for very rapid exhumation in the Dora Maira Massif, Western Alps. Lithos 41, 5–24.

Hanchar, J.M., Miller, C.F., 1993. Zircon zonation patterns as revealed by cathodoluminescence and backscattered electron images: implications for interpretation of complex crustal histories. Chem. Geol. 110, 1–13.

Hartmann, L.A., Leite, J.A.D., Silva, L.C. da, Remus, M.V.D., McNaughton, N.J., Groves, I.D., Fletcher, I., Santos, O.S., Vasconcellos, M.A.Z., 2000. Advances in SHRIMP geochronology and their impact on understanding the tectonic and metallogenic evolution of southern Brazil. Aust. J. Earth Sci. 47, 829–844.

Mantovani, S.M., Hawcksworth, C.J., Basei, M.A.S., 1987. Nd and Pb isotope studies bearing on the crustal evolution of the southeastern Brazil. Rev. Bras. Geocienc. 17 (3), 263–269.

Pitcher, W.S., 1983. Granite type and tectonic environment. In: Hsu, K.J. (Ed.), Mountain Building Processes. Academic Press, London, pp. 19–40.

Sheraton, J.W., Black, L.P., 1988. Chemical evolution of granitic rocks in the East Antarctic Shield, with particular reference to post-orogenic granites. Lithos 21, 37–52.

Silva, L.C. da, 1999. Geocronologia U–Pb SHRIMP e Sm–Nd na Província Mantiqueira meridional, no Cinturão Saldania (África do Sul) e a evolução do Ciclo Brasiliano/Pan-Africano. (PhD Thesis). Universidade Federal do Rio Grande do Sul-UFRGS. Porto Alegre, 243p (Unpublished).

Silva, L.C. da, Hartmann, L.A., McNaughton, N.J., Fletcher, I., 2000. Zircon U/Pb SHRIMP dates Neoproterozoic overprinting in Paleoproterozoic granitic-gneissic terranes, southern Brazil. Am. Mineral. 85, 649–667.

Silva, L.C. da, Armstrong, R., Pimentel, M.M., Scandolara, J., Ramgrab, G., Wildner, W., Angelim, L.A.A., Vasconcelos, A.M., Rizzoto, G., Quadros, M.L.E.S., Sander, A., Rosa, A.L.Z., 2002. Reavaliação da evolução geológica em terrenos pré-cambrianos brasileiros com base me novos dados U–Pb SHRIMP: Parte III. Províncias Borborema, Mantiqueira Meridional e Rio Negro-Juruena. Rev. Bras. Geocienc. 32 (4), 529–544.

Silva, L.C. da, McNaughton, N.J., Hartmann, L.A., Fletcher, I.R., 2003. Contrasting zircon growth patterns in Neoproterozoic granites in southern Brazil revealed by SHRIMP U–Pb analysis and SEM imaging: consequences for the discrimination of emplacement and inheritance ages (Preliminary Approach). In: 4st South America symposium on isotope geology, Salvador, 2003. Short papers, pp. 687–690.

Smith, J.B., Barley, M.E., Groves, D.I., Krapez, B., McNaughton, N.J., Bickle, M.J., Chapman, H.J., 1998. The Scholl shear zone, West Pilbara: evidence for a terrane boundary structure from integrated tectonic analyses, SHRIMP U–Pb dating and isotopic and geochemical data of granitoids. Precambrian Res. 88, 143–171.

Streckeisen, A., 1976. To each plutonic rock its proper name. Earth-Sci. Rev. 12, 1–33.

Vavra, G., Gebauer, D., Schmid, R., Compston, W., 1996. Multiple zircon growth and recrystallization during polyphase Late Carboniferous to Triassic metamorphism in granulites of the Ivrea Zone (Southern Alps): an ion microprobe (SHRIMP) study. Contrib. Mineral. Petrol. 122, 337–358.

Vavra, G., Schmid, R., Gebauer, D., 1999. Internal morphology, habit, and U–Th–Pb microanalyses of amphibolite- to granulite-facies zircons: geochronology of the Ivrea Zone (Southern Alps). Contrib. Mineral. Petrol. 134, 380–404.

Wahlen, J.B., Currie, K.L., Chappel, B.W., 1987. A type granites: geochemical characteristics, discriminations and petrogenesis. Contrib. Mineral. Petrol. 95, 407–419.

Williams, I.S., 1998. U–Pb geochronology by ion microprobe. In: McKibben, M.A., Shanks III, W.C., Ridley, N.I. (Eds.), Applications of microanalytical techniques to understanding mineralizing processes, Reviews in Economic Geology, vol. 7. Society of Economic Geology, pp. 1–35.